Thermoresponsive nanofibers loaded with antimicrobial ?-aminophosphonate-o/w emulsion supported by cellulose nanocrystals for smart wound care patches

International Journal of Biological Macromolecules 233 (2023) 123655

Contents lists available at ScienceDirect

International Journal of Biological Macromolecules

journal homepage: www.elsevier.com/locate/ijbiomac

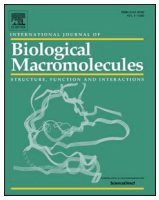

Thermoresponsive nanofibers loaded with antimicrobial α-aminophosphonate-o/w emulsion supported by cellulose nanocrystals for smart wound care patches

Dalia A. Elsherbiny [a,b], Abdelrahman M. Abdelgawad [c,d,*], Tharwat I. Shaheen [d], Nayera A.M. Abdelwahed [e], Stefan Jockenhoevel [b,f], Samaneh Ghazanfari [b,f,**]

[a] Chemistry Department, Faculty of Science, Menoufia University, Shebin El-Koom, Menoufia, Egypt
[b] Aachen-Maastricht Institute for Biobased Materials (AMIBM), Faculty of Science and Engineering, Maastricht University, Brightlands Chemelot Campus, Urmonderbaan 22, 6167 RD Geleen, the Netherlands
[c] Textile Research and Technology Institute, National Research Center (Affiliation ID: 60014618), 12622, Dokki, Giza, Egypt
[d] Chemistry Department, Faculty of Science, New Mansoura University, New Mansoura City 35511, Egypt
[e] Chemistry of Natural and Microbial Products Department, Pharmaceutical Industries Institute, National Research Centre, 12622, Dokki, Giza, Egypt
[f] Department of Biohybrid & Medical Textiles (BioTex), AME-Helmholtz Institute for Biomedical Engineering, RWTH Aachen University, Forckenbeckstrabe 55, 52072 Aachen, Germany

ARTICLE INFO

Keywords:
Antibacterial α-amino phosphonates
Thermoresponsive wound dressing
Electrospinning
Polybutylene succinate nanofibers

ABSTRACT

Long-term topical application of antibiotics on wounds has led to the emergence of drug-resistant bacterial infections. Antibiotic incorporation into the wound dressing requires enormous advancement of the field to ensure that the needed dose is released when the infection arises. This study synthesized a series of antimicrobial α-aminophosphonate derivatives, and the most effective compound was incorporated into thermoresponsive wound dressing patches. Wound dressing mats were fabricated by needleless electrospinning, and the resultant nanofiber mats were coated with a thermoresponsive eicosane/cellulose nanocrystals o/w system loaded with active α-aminophosphonate derivatives. Chemical, physical, thermal, and antimicrobial properties of the wound dressings were characterized wound dressings. Using SEM analysis, Nanofibers spun with 20 % w/v solutions were selected for drug-emulsion loading since they showed lower diameters with higher surface area.

Furthermore, the drug-emulsion coating on the electrospun dressings improved the hydrophilicity of the wound dressings, and the thermoresponsive behavior of the mats was proved using differential scanning calorimetry data. Finally, the drug-loaded electrospun meshes were found active against tested microorganisms, and clear inhibition zones were observed. In conclusion, this novel approach of synthesizing a new family of antimicrobial molecules and their incorporation into nanofibers from renewable sources exhibits great potential for smart and innovative dressings.

1. Introduction

Hospital-acquired infections (nosocomial infections) are the most common and severe complications affecting hospitalized patients. The infection causes many troubles to the patient, including local elevation of body temperature, and fever, for a long time which disturbs the vital processes in the body. Surgical wound infection accounts for most of the observed complications [1]. The adverse effect of these events influences >2 million patients annually in the USA alone, resulting in around 90,000 deaths and an estimated cost of $4.5 billion per year [2]. In addition, the use of traditional wound dressings and the available therapeutic options to treat infections are becoming insufficient due to increasing antibacterial resistance [3–5]. Therefore, much research is devoted to developing new antimicrobial agent classes. Among others,

* Correspondence to: A.M. Abdelgawad, Textile Research and Technology Institute, National Research Center (Affiliation ID: 60014618), 12622, Dokki, Giza, Egypt.
** Correspondence to: S. Ghazanfari, Department of Biohybrid & Medical Textiles (BioTex), AME-Helmholtz Institute for Biomedical Engineering, RWTH Aachen University, Forckenbeckstrabe 55, 52072 Aachen, Germany.
E-mail addresses: aabdelgawad2@gmail.com, aabdelg@ncsu.edu (A.M. Abdelgawad), Samaneh.ghazanfari@maastrichtuniversity.nl (S. Ghazanfari).

https://doi.org/10.1016/j.ijbiomac.2023.123655
Received 5 November 2022; Received in revised form 3 February 2023; Accepted 8 February 2023
Available online 11 February 2023

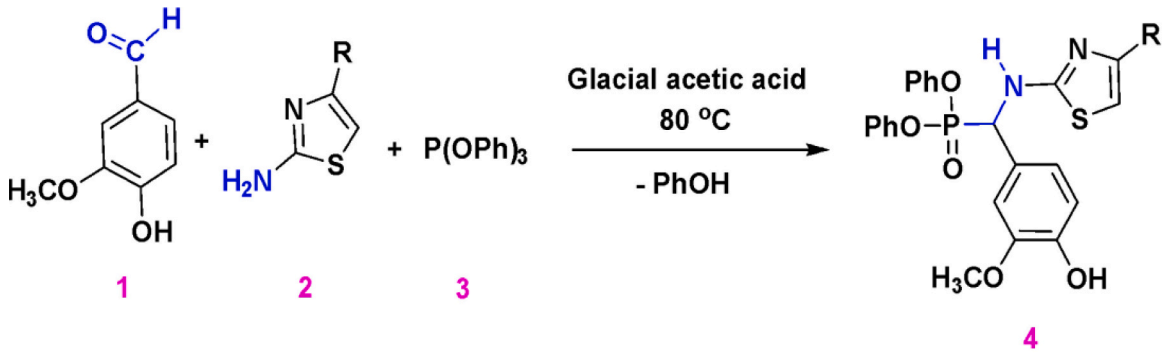

Compound No.	R	Compound No.	R
1 (4a)	**H**	4 (4d)	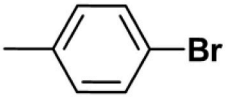
2 (4b)	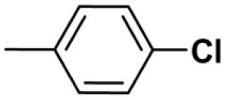		
3 (4c)	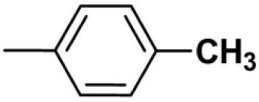	5 (4e)	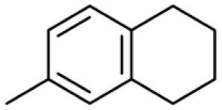

Scheme 1. Synthesis of α-aminophosphonates from vanillin, different amines, and triphenylphosphite

α-aminophosphonate compounds are recognized as unique pharmacophores from a drug design perspective and show promising biological activity against pathogens, metabolic stability, and negligible toxicity toward mammalian cells [6–10]. However, there is still a considerable gap to bridge and a continuous need to explore and design novel antimicrobial molecules that can be incorporated into wound dressings to overcome bacterial drug-resistance phenomena.

A wound dressing should protect the wound from the external environment and microbial invasion, absorb excess fluids and excaudate while maintaining a moist environment, and allow a degree of gas permeability for wound aeration [11]. It is also crucial that the dressing is lightweight and can be removed atraumatically to prevent further skin damage during dressing changes [12]. Conventional wound dressings, including cotton gauze [13] and viscose fabrics [14] are widely used; however, modern wound dressings such as thin films of hydrocolloids from alginate [15,16], chitosan [17], and collagen [18], as well as aerogels [19] and nanofibers [20–23] are emerging due to their unique properties and performance.

Nanofibers have a proven promising efficiency as innovative wound healing substrates due to their unique properties, such as, high surface area to volume ratio, high porosity and being lightweight [24,25]. In addition to their analogous physical properties to the extracellular matrix, nanofibers possess exceptional performances in cell adhesion, proliferation, and differentiation [26,27]. Furthermore, the nanofibers are prepared from renewable biobased sources, including polybutylene succinate (PBS) [28,29]. This has attracted significant attention in the last two decades due to their environmentally friendly properties, biocompatibility, and biodegradability. Furthermore, high throughput preparation of high-quality nanofibers has facilitated their use in the biomedical field.

Electrospinning (ES) is the most widely used method for preparing nanofibers due to its simplicity and economic feasibility [30,31]. Several electrospinning setups, including multi-jets from multi-needle and needleless systems, have been proposed for solution electrospinning to increase its productivity [32]. Needleless electrospinning technology has witnessed a remarkable development drive. It is available for industrial use, which allows the possibility of incorporating several active materials, such as antimicrobial agents and growth factors, into medicated and bioactive nanofiber dressings at large scale [33].

The inefficient use of antimicrobial agents, including medicated wound dressings, and the untimely control of infections have led to the emergence of multidrug-resistant bacterial strains, becoming a severe threat to public health [34]. Therefore, targeted delivery or intelligent systems are needed and thought to be a practical solution for such issues. Smart delivery systems allow direct active molecule transport to the infected site, boosting its availability and lowering cytotoxicity [35]. Engineered stimuli-responsive dry emulsions (oil/water) are one of the essential classes of smart drug delivery systems which use surfactants to stabilize droplets. Such emulsions respond to changes in external signals such as temperature and pH by solidifying or dissolution due to changes in the oil or water phase of the emulsion droplets [36].

Several organic and inorganic colloidal nanoparticles have been used to stabilize Pickering emulsions, such as chitin, starch, cellulose nanocrystals (CNC), silica, and clay as alternatives to traditional surfactants [37,38]. Biobased, sustainable polymers as surfactants are favored due to their abundance, sustainability, low cost, and low energy consumption [39]. Mainly, CNC is adsorbed irreversibly at the interface of water-oil; therefore, it has been efficiently used for developing oil/water emulsions that are relatively resistant to coalescence or sedimentation. This could be attributed to negatively charged sulfate ester groups on its

surface, which acquire electrostatic forces and suppress aggregation [40,41]. In addition to its stimuli-responsiveness properties, the Pickering emulsion systems can be used as a revisor or solubilization locus for large payloads of hydrophobic biomaterials, including drugs, in its oil phase [42].

Recently, eicosan (or icosane) was recognized as a thermoresponsive material. It is the shortest hydrocarbon compound in paraffin wax, with a melting temperature between 37 and 40 °C. Several researchers have developed dry emulsions using eicosan. For example, Deveci et al. developed an eicosan-based emulsion to prepare silk fibroin/chitosan microcapsules for high-load drug delivery applications [43]. Further, Umut Yucel et al. studied the distribution of solutes in eicosan o/w emulsions for food systems [44]. Recently, Shaheen et al. successfully prepared re-dispersible dry o/w emulsion-loaded antimicrobial silver, gold, and copper oxide nanoparticles to the eicosan/water system using eicosan as an oil phase and CNC as a stabilizing agent for the first time [45]. However, the loading of synthetic antimicrobial molecules has not been studied yet.

The current research has developed a thermoresponsive antimicrobial wound dressing patch made from polybutylene succinate nanofibers. The nanofiber mats were treated with a thermoresponsive eicosan/CNC o/w system loaded with newly synthesized and biologically active α-aminophosphonate derivatives. The system is designed to release its active molecule to the wound site only if an infection happens and the body's high temperature triggers the system. The nanofibers were produced via electrospinning using a semi-industrial scale needleless system (Elmarco™) and characterized by scanning electron microscopy (SEM). A series of amino phosphonates were synthesized, characterized, and their biological activity was screened against five human pathogenic microbial strains: *Escherichia coli* NRRL B-210 and *Klebsiella pneumonia* NCIMB 10341 as Gram -ve bacteria, *Bacillus subtilis* NRRL B-543 and *Staphylococcus aureus* NRRL B-313 as Gram +ve bacteria and the yeast *Candida albicans* NRRL Y-477. Afterward, the effective compound was loaded into the emulsion system. The drug-loaded emulsion was sprayed on one side of the nanofiber mats and left to dry under ambient conditions. The thermoresponsive properties of the system were studied by monitoring its thermal behavior using differential scanning calorimetry (DSC) measurements. Finally, the antimicrobial activity of the nanofiber patches was investigated. To our knowledge, no other work in the literature utilized the studied delivery system before.

2. Materials and methods

2.1. Materials

Solvents and chemicals required for synthesizing α-aminophosphonates, such as aminothiazoles, vanillin, triphenylphosphite, and acetic acid, were purchased from Sigma-Aldrich and. PBS fiber-grade resin (code: FZ78TM) was kindly provided by Mitsubishi Chemical Performance Polymer (MCPP), Dusseldorf, Germany. The melt flow rate of PBS was 22 g/10 min at 180 °C using a weight of 2.15 kg, and the crystalline melting temperature was 115 °C. For the preparation of thermoresponsive O/W emulsion, cellulose nanocrystals (CNC) were supplied from Celluforce, Inc., and eicosan (paraffin oil) was purchased from Sigma-Aldrich without any modification. Deionized water has been used in order to prepare solutions and suspensions.

2.2. Methods

2.2.1. Chemical synthesis of α-aminophosphonate derivatives

Five α-aminophosphonate compounds were prepared via a one-pot synthesis route as previously described [7]. Briefly, a mixture containing equimolar amounts of vanillin **1**, Amines **2**, and triphenylphosphite **3**, as shown in Scheme 1, in 5 mL of glacial acetic acid was kept under stirring at 80 °C for 8 h. The completion of the reaction was monitored by thin-layer chromatography (TLC) until all the starting components were used up. After completion of the reaction, the glacial acetic acid was evaporated, and the gummy residue was treated with diethyl ether to obtain solid particles. Finally, the precipitate was filtered off and crystallized from methylene chloride/ethyl acetate (1:2) to afford pure α-aminophosphonates derivatives in a good yield.

2.2.2. Thermo-responsive o/w emulsion

Thermo-responsive oil/water emulsion was prepared using eicosan as an oil liquid phase and CNC as a biosurfactant. In short, a constant ratio of eicosan: CNC (1:1) was used during the emulsification process. First, the eicosan was heated above its melting temperature (60 °C) and mixed with CNC in a plastic tube. Then a specific volume of warmed distilled water was added to reach an o/w ratio of 20: 80 under a vortex shaker. Following this, the mixture was sonicated for 20 s using an ultrasonic device with a dipping titanium probe close to the emulsion surface.

2.2.3. Drug-loaded eicosan/CNC emulsion

For the thermo-responsive o/w emulsion-loaded drug, the antimicrobial activity of the synthesized α-aminophosphonates was screened, and the most effective compound was further incorporated into the emulsion formation. The oil phase consists of the α-aminophosphonate compound dissolved in the molten eicosan at a typical ratio of 1:2. The latter oil phase was then used for emulsification, according to the earlier step.

2.2.4. PBS fiber formation via electrospinning and drug emulsion loading

PBS polymer was dissolved in chloroform and prepared in four different concentrations (15, 20, 25, and 30 % w/v). The electrospinning was carried out using a high throughput needle-free electrospinning system (Nanospider™ by Elmarco, Czech Republic). The spinning process starts by connecting the high-voltage power supply electrode conductive stationary wire electrode. The spinning solution was fed from a 50 mL container with a rate of 5 mL/h. Next, a designated electrical potential (25 kV) was applied over a fixed distance of 25 cm between the wire and the collector. The samples were collected on a polypropylene nonwoven fabric sheet. Several samples were collected for 10 min and kept for morphological characterization; on the other hand, the remaining samples were collected for 6 h. Finally, the samples were removed from the spinning collector and always kept under vacuum for additional characterization.

2.3. Characterization

2.3.1. Chemical structure of synthesized molecules

Proton Nuclear Magnetic Resonance (^{1}H NMR) and Carbon-13 nuclear magnetic resonance (^{13}C NMR) measurements (using DMSO-d_6 as solvent) were executed using a Varian and Bruker Avance (USA), 500 MHz. Fourier Transform Infrared spectroscopy (FTIR) spectroscopy was done using Thermo Nicolet instrument (USA). Chemical changes that happened concerning the respective solvent were documented in ppm. The Chemical shifts (δ) were recorded in parts per million (ppm) relative to the appropriate solvent as the internal standard. Standard abbreviations were documented (b → broad; s → singlet; d → doublet; m → multiplet). Additionally, mass spectroscopy measurements were performed to determine the purities of the obtained compounds using Shimadzu QL-800 (15-70 V) instrument. Thin Layer Chromatography (TLC) plates on Kiesel gel (F254, Merck) were used to control and monitor the progress of the reaction.

2.3.2. Antibacterial screening of aminophosphonate derivatives

Antimicrobial assay of different synthesized aminophosphonate compounds was performed in vitro using the agar well-diffusion method in Mueller Hinton agar (MHA) plates, as described by Das et al. [46], against five human pathogenic microbial strains: *Escherichia coli* NRRL B-210 and *Klebsiella pneumonia* NCIMB 10341 as Gram -ve bacteria,

Bacillus subtilis NRRL B-543 and *Staphylococcus aureus* NRRL B-313 as Gram +ve bacteria, and the yeast *Candida albicans* NRRL Y-477.

A 0.5 mL suspension from each microorganism (giving a final inoculum of 1–2 × 10^8 CFU/mL) mentioned above was added to a sterile MHA plate at 40 °C and allowed to solidify for 30 min. Identical cuts (holes, 7 mm) in diameter were made using a cork borer tool. Precisely, 0.1 mL of the prepared aminophosphonate compound samples from a stock solution of 100 μg/mL dissolved in dimethylsulphoxide DMSO were added inside the holes. The control hole was filled with DMSO alone. The inoculated plates were left for one hour at room temperature before incubation to allow active material diffusion and minimize the effects of time variation between the applications of the different solutions. The previous procedure was performed using the Sabouraud dextrose agar medium on *Candida albicans* NRRL Y- 477. All inoculated plates were incubated at 36 °C for 24 h and monitored for antimicrobial activity. The inhibition zone diameters were measured and related to the standard antibiotics fluconazole (100 units/mL) and Ciprofloxacin (100 μg/mL) for antifungal and antibacterial activity, respectively.

In further investigation, PBS nanofiber membrane discs of 23 mm diameter loaded with the most biologically active (antimicrobial) aminophosphonate compound and their efficiency were investigated against the above-mentioned pathogenic microorganisms and compared with unloaded PBS membrane as a control. Incubation of the treated membrane at 40 °C for one hour is recommended before loading to the sterile MHA plates containing the tested microorganisms to ensure the release of the loaded drug.

2.3.3. Antimicrobial efficacy of aminophosphonates: determination of the minimum inhibitory concentration (MIC)

The micro broth dilution method determined the synthesized aminophosphonate compounds' minimum inhibitory concentration (MIC). For MIC, serial dilutions of the samples were prepared (100, 50, 25, 10, and 5 mg/mL). The microbial suspensions were used as a positive control, and synthesized aminophosphonate compounds in broth were used as a negative control. Incubation of the tubes was carried out at 37^o C for 24 h for the pathogenic microorganisms and was observed for any visible growth. The positive control contained Ciprofloxacin for bacteria and fluconazole for yeast as a standard drug at 5 to 0.1 μg/mL concentrations. Therefore, the MIC was interpreted as the lowest concentration of the synthesized aminophosphonate compounds that showed no visible growth compared to control tubes containing only the synthesized aminophosphonate compounds [47]. A UV–vis spectrophotometer (Agilent technologies Cary 100 series) was used to measure the growth of microorganisms by measuring the turbidity at 600 nm after 24 h of incubation (Table 2). The experimental results were expressed as three replicates' mean ± standard deviation (SD).

2.3.4. Fiber surface morphology

The morphology of fibers was investigated using JEOL-6400F, Field Emission Scanning Electron Microscope (FE-SEM) equipped with an X-ray detector. The SEM instrument functioned at 10 kV and 20 mm working distance. The nanofiber sample was fixed on conductive-carbon tape, followed by coating a gold/palladium layer (5 nm).

2.3.5. Fiber wettability: water contact angle and equilibrium absorbency

The water contact angle technique was employed to investigate the electrospun PBS nanofibers' hydrophilicity/hydrophobicity. An automatic micro-syringe was used at an 8–12 drop/min; water drops (38 °C) were visualized under a microscope attached to a Phoenix-SEO camera. Image-XPFW012108 and Image-J1.410 software was utilized to process the images.

The equilibrium absorbency test was executed to evaluate the absorption effectiveness of PBS nanofibers upon free swelling for 12 h at 38 °C. First, the dry weight (W1) was recorded, and the samples were then positioned in a Petri dish filled with PBS solution (pH 7) and stored for 24 h. Finally, a paper tissue was used to remove excess water from the sample's surface, and the swollen samples were weighed (W2).

Equilibrium absorbency was calculated from the following formula:

$$EA\ (\%) = [(W2 - W1)/W1] \times 100$$

where EA is the percentage of free absorbency.

2.3.6. Drug-loaded o/w eicosan emulsion and fiber interaction

The average emulsion droplet diameter size was measured by laser light scattering using a particle size distribution analyzer (Horiba LA-960, Japan). The refractive indexes used were 1.44 and 1.33 for eicosan and water, respectively. At the same time, the surface morphology of the emulsion was visualized after lyophilizing using a freeze drier at −60 °C. The dried emulsion was then monitored using a JEOL JSM-7600F field-emission scanning transmission electron microscopy (STEM).

To effectively investigate the changes in chemical structures of CNC and the thermos-responsive o/w emulsion with and without drug loading, the FTIR using S-100 spectrometer (PerkinElmer-USA) analysis was used. While the change in their crystal structure was examined using X-ray diffraction (XRD) patterns (Philips PW3040 powder X-Ray diffractometer). SEM was also used for surface morphological characterization of drug encapsulated o/w eicosan emulsion and PBS nanofibers loaded drug/eicosan emulsion.

2.3.7. The thermoresponsive drug release profile

The influence of thermal trigger on the release profile of PBS nanofibers loaded with α-aminophosphonate O/W eicosan emulsion was determined by monitoring the melting endotherm using DSC (DSC Q100; TA Instruments, USA). In addition, the emulsion dissociation temperature point was precisely monitored by investigating the behavior of blank PBS nanofibers, drug emulsion, and drug-emulsion-loaded fibers.

3. Results and discussion

The ultimate goal of the current study is to develop a smart medicated wound dressing that can release drugs upon the change in body temperature. Such thermoresponsive patches were made from biobased nanofibers, PBS, through electrospinning and exhibited lightweight, high surface area, and durable standalone performance. In addition, a series of α-aminophosphonate compounds were prepared and characterized, and their antimicrobial activity was screened against the most commonly found pathogens in the infected wounds. Further, the most potent compound was formulated with an eicosan/CNC system to form a sTable o/w thermoresponsive emulsion. Finally, the properties of the developed patches were investigated, and the results are presented below.

3.1. Synthesis of α-aminophosphonate derivatives

Several synthetic routes were recorded in the literature for synthesizing α-aminophosphonates [48]. A simple and efficient method for synthesizing α-Aminophosphonates was developed for the first time in a one-pot procedure using aldehyde, aniline, and triphenyl phosphite in the presence of acetic acid as a catalyst and solvent [10,49]. In the present research, new α-aminophosphonates derivatives have been prepared using the above methodology. Vanillin was incorporated as a base aldehyde, and five different amines were used in the synthesis. The chemical structures of the synthesized compounds α-aminophosphonates (listed in scheme 1) were interpreted and investigated by several techniques such as IR, ^{1}H NMR, ^{13}C NMR, ^{31}P NMR, and mass spectrometry. Real-time charts can be found in the supporting documents.

Table 1
In vitro antimicrobial activity of aminophosphonate drugs by agar diffusion method.

Compound	Microorganism inhibition zone diameter (mm)				
	Gram +ve bacteria		Gram –ve bacteria		Yeast
	Bacillus subtilis	*Staphylococcus aureus*	*Escherichia coli*	*Klebsiella pneumonia*	*Candida albicans*
1 (4a)	19 ± 0.95	12 ± 0.6	18 ± 0.9	12 ± 0.6	20 ± 1
2 (4b)	20 ± 1	12 ± 0.6	18 ± 0.9	11 ± 0.55	18 ± 0.9
3 (4c)	19 ± 0.95	12 ± 0.6	19 ± 0.95	13 ± 0.65	21 ± 1.05
4 (4d)	17 ± 0.85	13 ± 0.65	14 ± 0.7	13 ± 0.65	20 ± 1
5 (4e)	18 ± 0.9	12 ± 0.6	15 ± 0.75	11 ± 0.55	19 ± 0.95
Ciprofloxacin	28 ± 1.4	28 ± 1.4	25 ± 1.25	33 ± 1.65	-ve
Fluconazole	-ve	-ve	-ve	-ve	30 ± 1.5

Highly active = (inhibition zone ≥20 mm) Moderately active = (inhibition zone 14–19 mm).
Slightly active = (inhibition zone 8–13 mm) Inactive (−ve) = no inhibition zone.

3.1.1. Diphenyl ((4-hydroxy-3-methoxyphenyl)(thiazol-2-ylamino) methyl)phosphonate (1, 4a)

Orange color, Yield (95 %), FTIR, (cm^{-1}): 3230–3560 (br., NH, OH), 1595 (C═C, Ar.), 1269 (P=O), 758 (P-C). ^{1}H NMR (DMSO-d_6 500 MHz, ppm) δ: 7.94–6.57 (m, 15H), 5.65 (s, 1H, NH), 4.99 (d, J = 27.0, 1H, NCHP), 3.69 (s, 3H, OCH3). ^{13}CNMR (DMSO-d_6 500 MHz, ppm) δ:- 157.78, 150.35, 147.92, 147.49, 130.17, 129.83, 125.61, 123.68, 120.73, 119.26, 115.70, 115.23, 65.38, 56.03. ^{31}P NMR (500 MHz, DMSO, ppm) δ: 17.59. LCMS, m/z ($C_{23}H_{21}N_2O_5PS$) calcd, 468.46; found, 469.05 [M + 1] $^{+}$.

3.1.2. Diphenyl (((4-(4-chlorophenyl)thiazol-2-yl)amino)(4-hydroxy-3-methoxyphenyl)methyl)phosphonate (2, 4b)

Gray color, Yield: 96 %, FTIR (cm^{-1}): 3215–3550 (br., NH, OH), 1595 (C═C, Ar.), 1267 (P=O), 825 (C-Cl), 759 (P-C). ^{1}H NMR (DMSO-d_6 500 MHz, ppm) δ:- 8.01–6.53 (m, 18H), 5.66 (s, 1H, NH), 4.98 (d, J = 30.2, 1H, NCHP), 3.69 (s, 3H, OCH3). ^{13}C NMR (DMSO-d_6 500 MHz, ppm) δ = 157.78, 150.35, 147.92, 147.49, 130.37, 130.17, 129.83, 129.51, 125.69, 123.68, 120.99, 120.73, 119.26, 116.06, 115.70, 115.23, 65.38, 56.03. ^{31}P NMR (500 MHz, DMSO, ppm) δ: 17.38; LCMS, m/z ($C_{29}H_{24}ClN_2O_5PS$) calcd, 579.00; found, 579.99 [M + 1]$^{+}$.

3.1.3. Diphenyl ((4-hydroxy-3-methoxyphenyl)((4-(p-tolyl)thiazol-2-yl) amino)methyl)phosphonate (3, 4c)

Light purple color, Yield (94 %), FTIR (KBr) cm^{-1}:- 3217–3540 (br., NH, OH), 1597 (C═C, Ar.), 1265 (P=O), 758 (P-C). ^{1}HNMR (DMSO-d_6 500 MHz, ppm) δ:- 8.15–6.67 (m, 18H. Ar-H), 5.91 (s, 1H, NH), 5.24 (d, J = 26.8, 1H, NCHP), 3.94 (s, 3H, OCH3), 2.74 (s, 3H, CH3). ^{13}CNMR (DMSO-d_6 500 MHz, ppm) δ: δ = 172.50, 157.80, 150.29, 148.08, 130.34, 130.19, 129.82, 129.59, 129.28, 128.79, 128.25, 125.68, 121.02, 120.56, 119.25, 115.70, 65.38, 56.16, 21.51. ^{31}P NMR (500 MHz, DMSO, ppm) δ: 16.26. LCMS, m/z ($C_{30}H_{27}N_2O_5PS$) calcd, 558.59; found, 559.50 [M + 1] $^{+}$.

3.1.4. Diphenyl (((4-(4-bromophenyl)thiazol-2-yl)amino)(4-hydroxy-3-methoxyphenyl)methyl)phosphonate (4, 4d)

Gray color, Yield (95 %), FTIR (KBr) cm^{-1}:- 3246–3555 (br., NH, OH), 1593 (C═C, Ar), 1269 (P=O), 758 (P-C), 686 (C-Br). ^{1}HNMR (DMSO-d_6 500 MHz, ppm) δ:- 8.13–6.24 (m, 18H, Ar-H), 5.66 (s, 1H, NH), 4.99 (d, J = 27.0, 1H, NCHP), 3.69 (s, 3H, OCH3). ^{13}CNMR (DMSO-d_6 500 MHz, ppm) δ: 155.70, 152.88, 148.20, 145.97, 128.09, 127.72, 127.48, 127.16, 126.67, 126.15, 123.55, 118.46, 117.15, 116.44, 113.60, 110.95, 63.28, 54.06. ^{31}P NMR (500 MHz, DMSO, ppm) δ: 15.80; LCMS, m/z ($C_{29}H_{24}BrN_2O_5PS$) calcd, 623.46; found, 621.99 [M-1]$^{-}$.

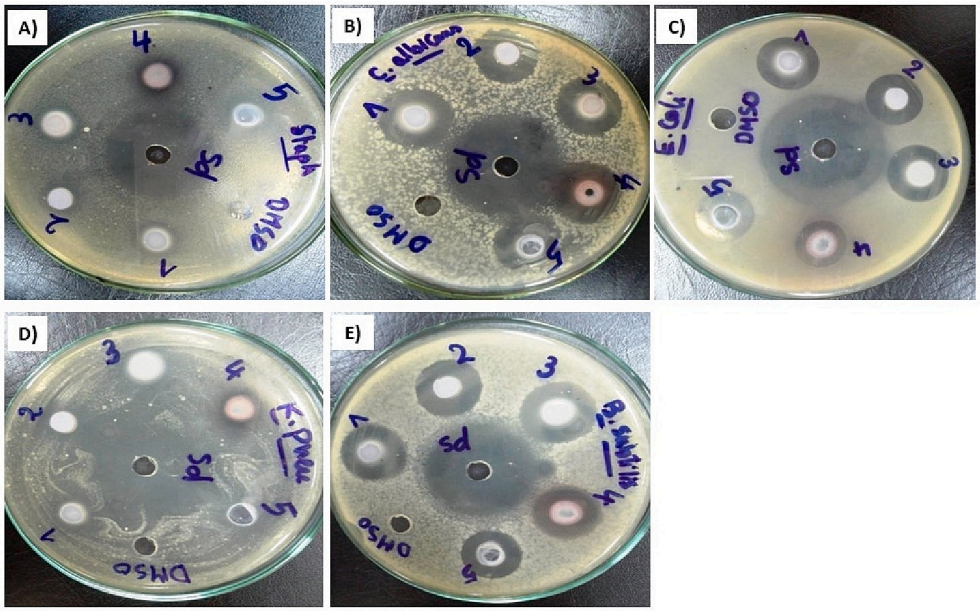

Fig. 1. In vitro antimicrobial activity of aminophosphonate drugs via inhibition zone method. A) *Staphylococcus aureus*, B) *Candida albicans*, D) *E. coli*, D) Klebsiella pneumonia*, and E) Bacillus subtilis.*

Table 2
MIC of the synthesized aminophosphonate compounds (mg/mL) against tested microorganisms.

Compound	MIC (mg/mL)				
	Gram +ve bacteria		Gram –ve bacteria		Yeast
	Bacillus subtilis	*Staphylococcus aureus*	*Escherichia coli*	*Klebsiella pneumonia*	*Candida albicans*
1 (4a)	0.914 ± 0.04600.00.0460.046±	1.44 ± 0.072	0.99 ± 0.05	1.44 ± 0.072	0.83 ± 0.041
2 (4b)	0.83 ± 0.041	1.440.072±	0.99 ± 0.05	1.52 ± 0.076	0.99 ± 0.05
3 (4c)	0.914 ± 0.046	1.42 ± 0.07	0.9140.045	1.37 ± 0.068	0.609 ± 0.030
4 (4d)	1.06 ± 0.053	1.37 ± 0.068	1.29 ± 0.064	1.37 ± 0.068	0.83 ± 0.041
5 (4e)	0.99 ± 0.04	1.44 ± 0.072	1.14 ± 0.072	1.52 ± 0.076	0.91 ± 0.046
Ciprofloxacin	0.72 ± 0.04	0.7 ± 0.035	0.812 ± 0.04	0.421 ± 0.02	-ve
Fluconazole	-ve	-ve	-ve	-ve	0.51 ± 0.025

3.1.5. Diphenyl ((4-hydroxy-3-methoxyphenyl) ((4-(5,6,7,8-tetrahydronaphthalen-2-yl)thiazol-2-yl)amino)methyl)phosphonate (5, 4e)

Gray color, Yield (93 %), IR (KBr)cm^{-1}: 3220–3550 (br., NH, OH), 1595 (C═C, Ar.), 1269 (P═O), 758 (P-C). ^{1}HNMR (DMSO-d_6 400 MHz, ppm) δ: 8.30–6.84 (m, 17H), 6.11 (s, 1H, NH), 5.45 (d, J = 26.9, 1H, NCHP), 4.15 (s, 3H, OCH_3), 3.22–2.81 (m, 4H), 2.28–1.98 (m, 4H). ^{13}CNMR (DMSO-d_6 500 MHz, ppm) δ: 172.47, 166.99, 157.80, 148.07, 137.13, 136.88, 132.13, 130.32, 130.17, 129.95, 129.81, 129.19, 129.05, 125.61, 121.00, 120.54, 119.24, 115.69, 65.38, 56.15, 29.01, 23.13. ^{31}P NMR (500 MHz, DMSO, ppm) δ: 17.41. LCMS, m/z ($C_{33}H_{31}N_2O_5PS$) calcd, 598.65; found, 599.55 [M + 1] $^{+}$.

3.1.6. Antibacterial screening of aminophosphonate derivatives

The synthesized aminophosphonate compounds showed varying degrees of growth inhibition against the tested microorganisms. The results are presented in Table 1, and the best antibacterial activity was 3 (4c), followed by compounds 2 (4b), 1(4a), 4 (4d), and 5 (4e). The antifungal activities depicted in Table 1 revealed that compounds 3 (4c), 1(4a), and 4 (4d) showed potent activity against *Candida albicans,* followed by compounds 5 (4e) and 2 (4b), which showed moderate activity. However, compound 2 (4b) displayed intense activity against *Bacillus subtilis,* followed by compounds 1 (4a) and 3 (4c), 5 (4e), and 4 (4d) revealed suiTable activities. Finally, compound 4 (4d) showed good activity against *Staphylococcus aureus,* followed by all other compounds. Several studies stated that α-amino-phosphonates have antibacterial and antifungal activities regardless of the moiety [8]. So, most of these compounds can be considered broad-spectrum potential antimicrobial agents.

Fig. 1 shows the agar Petri dishes of the tested compounds against A) *Staphylococcus aureus*, B) *Candida albicans*, D) *E. coli*, D) *Klebsiella pneumonia*, and E) *Bacillus subtilis*. The disc in the middle of the dish represents the reference antibiotic (Ciprofloxacin) or the antifungal agent (Fluconazole). The tolyl derivative of the aminophosphonate molecule, 3 (4c), showed broad spectrum activity against the five tested microorganisms. Therefore, it was selected as the most potent compound for fiber emulsion formation and loading to nanofiber patches.

3.2. The minimum inhibitory concentration of aminophosphonate derivatives

The minimum inhibitory concentration of the synthesized compounds was studied and referenced to the commonly used antimicrobial agents Ciprofloxacin and Fluconazole drugs (Table 2). The tolyl derivative, 3 (4c), showed MIC striking results against *Bacillus subtilis* (0.91 mg/mL) and *Escherichia coli* (0.91 mg/mL), close to that of the reference antibiotic Ciprofloxacin (0.72 mg/mL) and (0.81 mg/mL), respectively. Further, it showed its lowest MIC value against *Candida albicans* (0.60 mg/mL) compared to the reference Fluconazole (51 mg/mL). On the other hand, it showed a relatively high MIC value against *Staphylococcus aureus* (1.42 mg/mL) compared to (0.7 mg/mL) for Ciprofloxacin. On

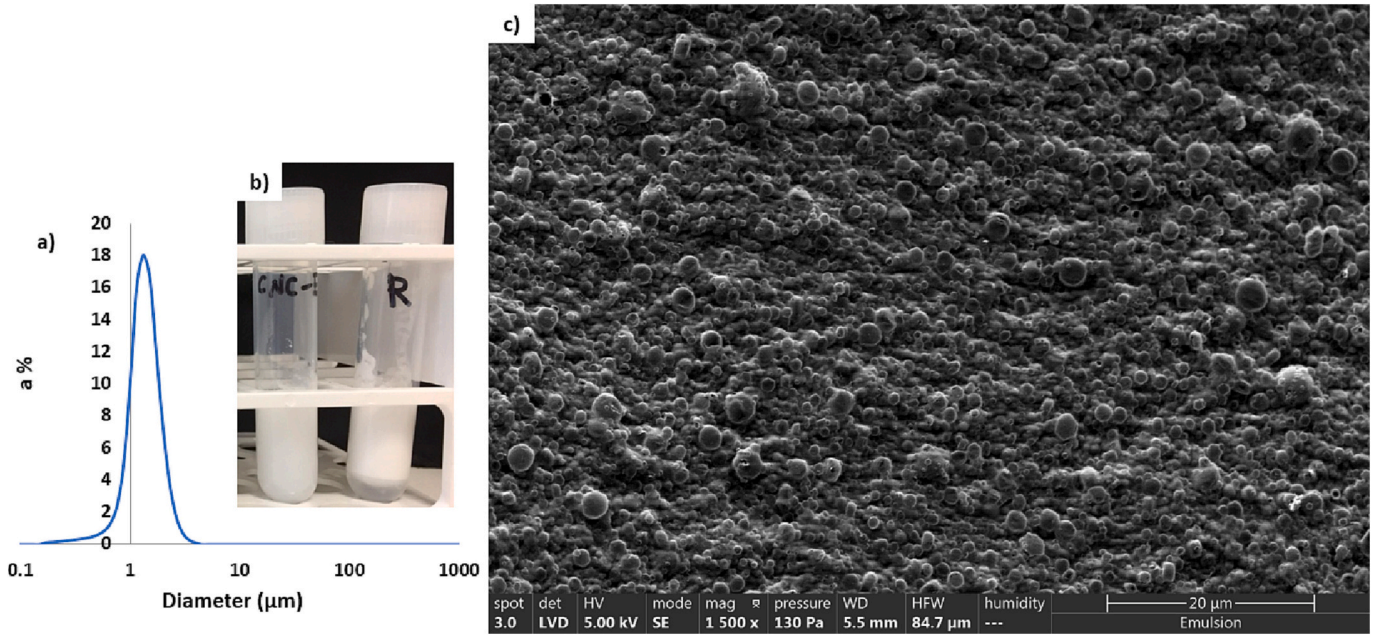

Fig. 2. a) Average diameter distribution of emulsion droplets measured by dynamic light scattering, b) photo of emulsion stabilized by CNC (tube to the left) and the unsTable reference sample (tube to the right), c) TEM image of the as-prepared o/w eicosan emulsion stabilized-CNC after freeze-drying and B) droplet size distributions, including a photographic picture of the obtained emulsion.

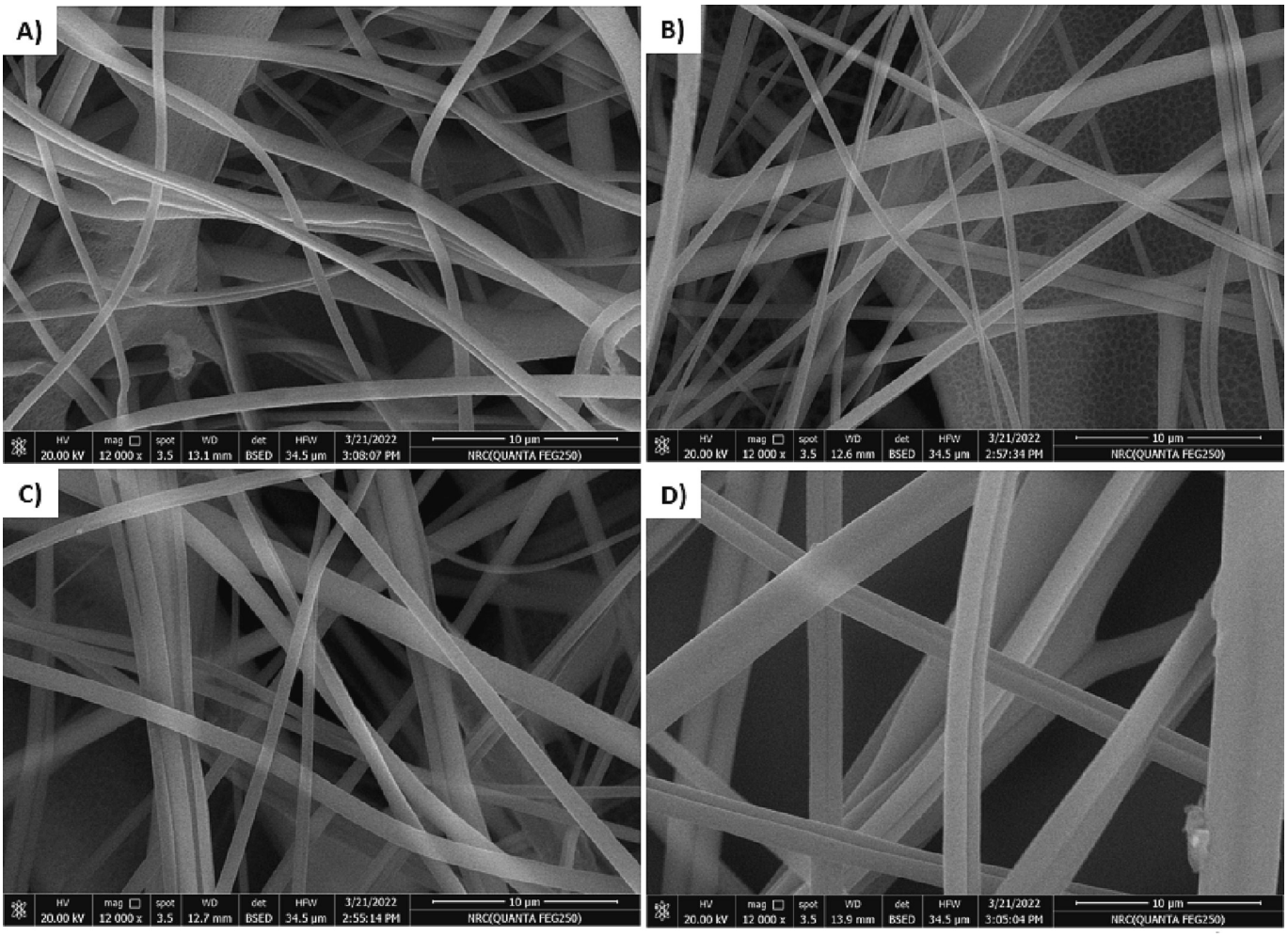

Fig. 3. SEM micrographs of PBS nanofibers at different polymer concentrations; A) 15 % w/v, B) 20 % w/v, C) 25 % w/v, and D) 30 % w/v in chloroform.

the other hand, derivatives showed slightly higher MIC against the tested microorganisms.

3.3. Emulsion stability and characterizations

Regarding the amphiphilic character of cellulosic materials, CNC was harnessed successfully for stabilizing eicosan o/w emulsion, as clearly pointed out in Fig. 2. In addition, the prepared emulsion had a milky color referring to the formation of Pickering emulsion with the mean diameter size lying in the range of 1–1.25 μm as shown in Fig. 2-a. Besides, the emulsion showed high stability over one month (Fig. 2-b) compared with a reference emulsion formulation. Moreover, STEM (Fig. 2-c) showed spherical droplets with a homogenous size distribution, indicating CNC's capability to stabilize the formed o/w emulsion well, especially after lyophilization when the water is removed.

The re-desperation of dried eicosan emulsion in the water had no significant influence on the size of droplets. Hence, it declared that CNC surrounds the eicosan oil droplets, which, in turn, stabilizes the droplets by dint of their surface amphiphilic properties that maintain the repulsion force between the oil droplets unchanged [45].

3.3.1. Fiber surface morphology

Nanofibers from PBS were fabricated via electrospinning using a high-throughput needle-free system (Nanospider). The electrospinning of PBS is already established in the literature [50–52] using the traditional syringe-pump setup; however, spinning via a high throughput needle-free system was not investigated before. Therefore, nanofiber formation was optimized by studying four PBS solutions with different concentrations (15, 20, 25, and 30 % w/v). Fig. 3 shows the SEM micrographs of the spun fibers. The average fiber diameter increased by increasing the concentration of PBS in the solution. The electrospinning process using 15 % w/v PBS concentration (Fig. 3-A) was not sTable; this may be attributed to the low viscosity of the solution and the high rate of solvent (chloroform) evaporation. Samples of 20 % w/v (Fig. 3-B) and 25 % w/v (Fig. 3-C) produced a standalone nanofiber mat with average diameters of 250 nm and 350 nm, respectively. Nevertheless, a further increase in the concentration (30 % w/v) (Fig. 3-D) produced fibers with larger diameters (average 550 nm) and led to solution solidification prior to spinning. Therefore, the PBS concentration of 20 % w/v was selected for drug-emulsion loading since it produced nanofibers with lower diameters and expected higher surface area [53].

For drug-emulsion loading, a large nanofiber sheet (30 × 60 cm) was produced via the deposition of PBS for 3 h. The nanofiber sheet was made using 100 mL PBS solution coated with the designated drug-emulsion formulation (total volume, 10 mL). Fig. 4 (A) shows the freeze-dried drug-emulsion particles. It is clear that the particles had a spherical shape and were still in the micrometer range (1–1.5 μm) after drug loading. Uncoated PBS nanofibers are presented in Fig. 4 (B), and the coated drug-emulsion formulation is presented in Fig. 4 (C) and Fig. 4 (D) with higher magnification. It is indicated that the drug-loaded emulsion was deposited on the fiber surface evenly.

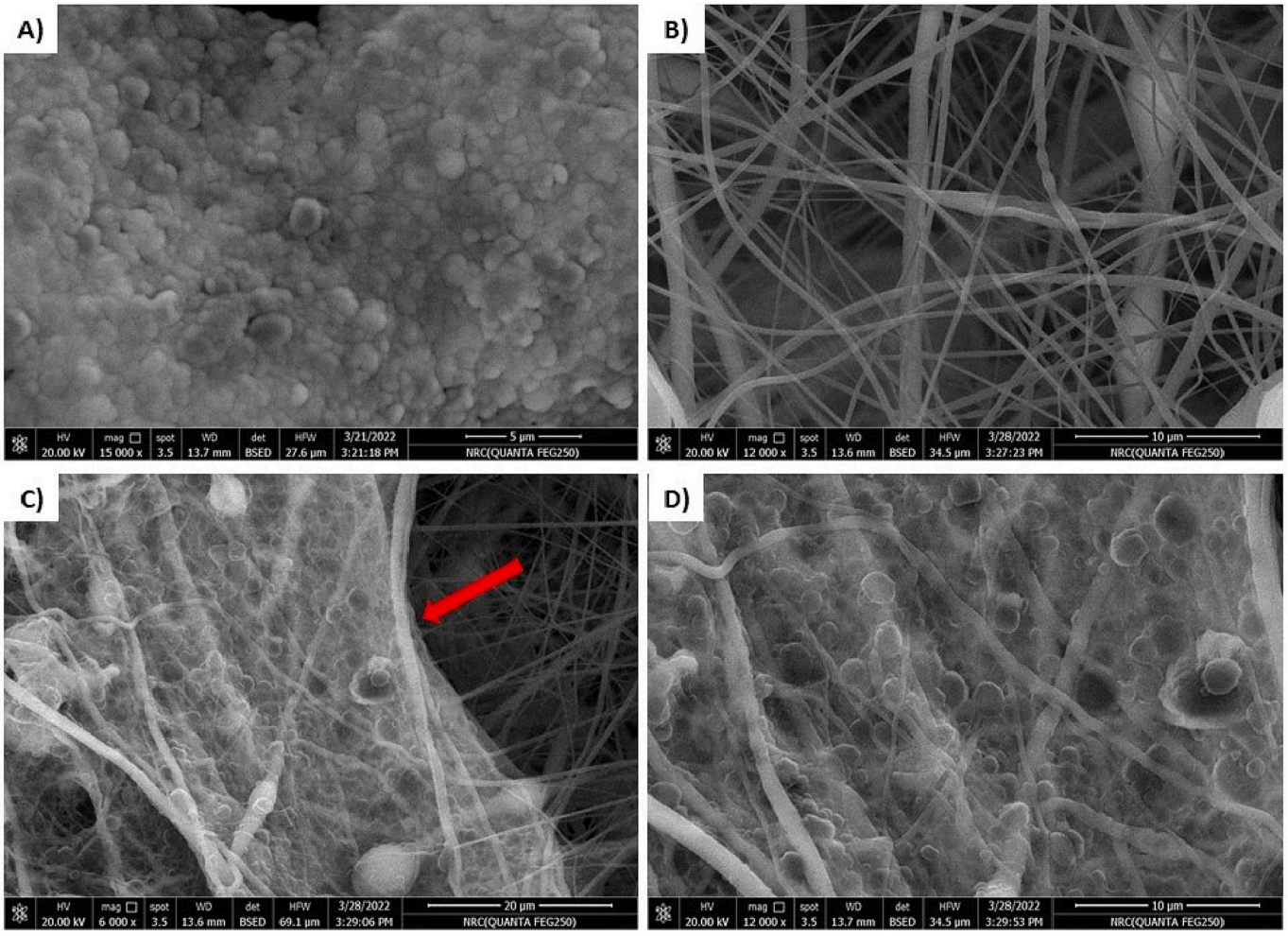

Fig. 4. SEM micrographs of A) drug loaded-emulsion particles, B) untreated PBS nanofibers produced at 25 % w/v polymer concentration, C) PBS nanofibers coated with drug-emulsion and the red arrow points at the deposited layer, D) higher magnification of the pointed area in image C. (For interpretation of the references to color in this figure legend, the reader is referred to the web version of this article.)

3.4. Fiber wettability: water contact angle and equilibrium absorbency

The change in hydrophilicity of the drug-emulsion loaded and blank PBS nanofibers were tested, and the results are presented in Fig. 5. The water contact angle of untreated PBS nanofibers was 137.3° (Fig. 5-A), which suggests a hydrophobic nature [54]. However, when the fibers were coated with the drug emulsion, the water contact angle dropped to 88.4° (Fig. 5-B). This may be attributed to the melting of eicosan molecules due to the use of the warm buffer (38 °C) in the measurement and the presence of CNC in the emulsion formulation. Both measurements were recorded after 5 s of drop/fiber contact. The water contact angle of coated fibers was further monitored at 10 (Fig. 5-C) and 20 s (Fig. 5-D). The contact angle value drooped to 69.6° after 10 s and could not be measured after 20 s, which indicated improved fiber wettability and gradual water uptake over time. Such hydrophilization effect of CNC was observed before [55].

The equilibrium absorbency of the blank and drug-emulsion coated nanofibers was estimated after 12 h of impregnation in the buffer solution (38 °C), and the percentage of absorbency was 25 % and 41 % of the sample's original weight, respectively. The results suggest that blank PBS fibers could host fluids inside the nanofiber mat's pores and that the coated fibers' improved wettability could be attributed to the presence of CNC residuals on the surface.

3.5. Drug-loading and interaction with PBS nanofibers: FTIR and XRD

Fig. 6 presents the FTIR chart of the PBS nanofibers, drug emulsion, and nanofiber loaded with drug emulsion. In the spectra of nanofiber loaded with drug emulsion, the broadband between 3593 cm^{-1} and 3082 cm^{-1} corresponds to –OH of CNC and -OH and –NH groups of the drug compound. Also, the absorption band assigned at 2954 cm^{-1}, 2909 $cm^{-1,}$ and 2849 cm^{-1} corresponds to the –CH stretching vibration of eicosan [56]. The band at 2947 cm^{-1} is related to –CH stretching of PBS, indicating that the drug emulsion was loaded on the PBS nanofiber. The absorption band assigned at 1716 cm^{-1} corresponds to the carbonyl C═O stretching vibration of the ester group of PBS. Additionally, the peak at 1332 cm^{-1} is the characteristic of –COO- bond stretching vibration [57]. The assigned band at 1158 cm^{-1} belongs to the repeated unit's C–O–C stretching vibration (–OCH_2CH_2). However, the intensity of the peaks at 1716 cm^{-1}, 1332 $cm^{-1,}$ and 1158 cm^{-1} decreased compared to the peaks of PBS nanofiber, indicating that hydrogen bonding was formed between the drug emulsion and the PBS fiber [58]. The results indicate the successful loading of the drug emulsion onto the fiber surface and the presence of a physical binding interaction.

Fig. 7 represents XRD patterns of PBS nanofibers, eicosan O/W emulsion, and drug-loaded PBS nanofibers. It can be seen that the XRD patterns of PBS nanofibers manifested the prominent characteristic peaks of the semi-crystalline phase at $2\theta = 19.5°$, 22.4°, and 29.1°[59]. Further, the XRD of eicosan O/W emulsion appeared to have a typical

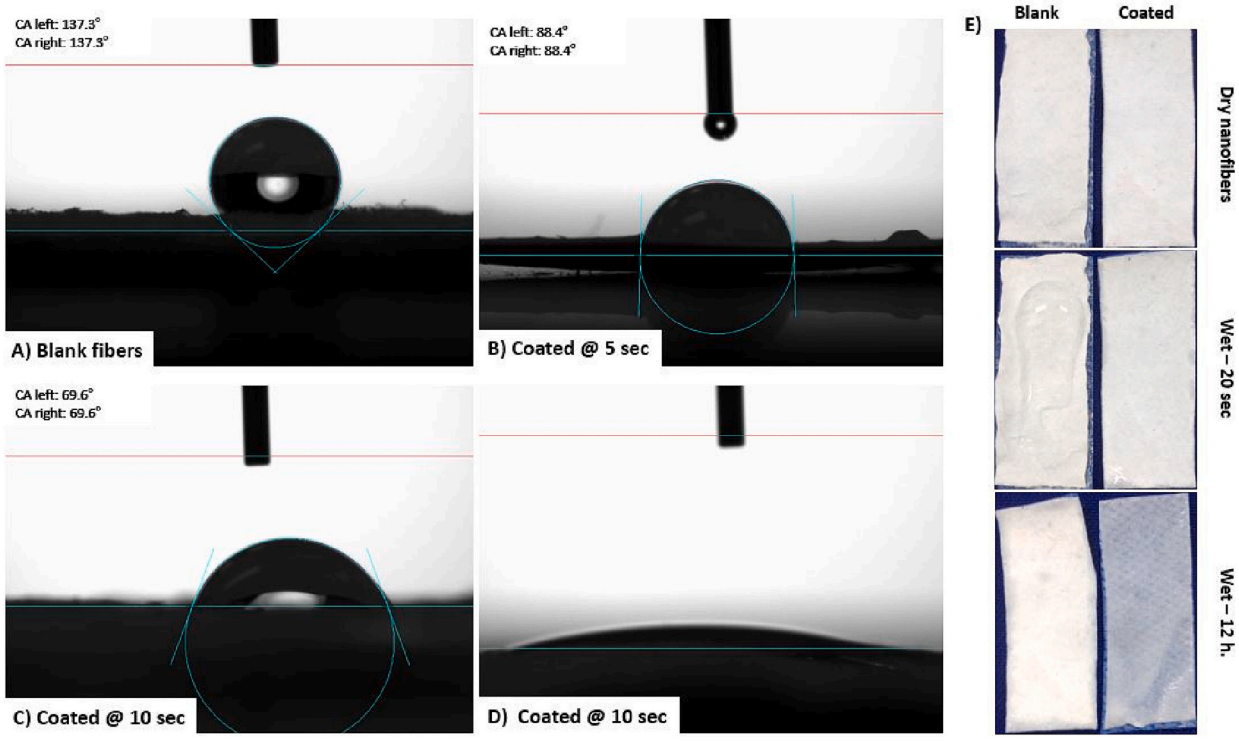

Fig. 5. Contact angle (CA) of drug-loaded fibers. A) blank PBS nanofibers after 10 s, B) drug-emulsion-loaded nanofibers after 5 s, C) drug-emulsion-loaded nanofibers after 7 s, and D) drug-emulsion loaded nanofibers after 10 s.

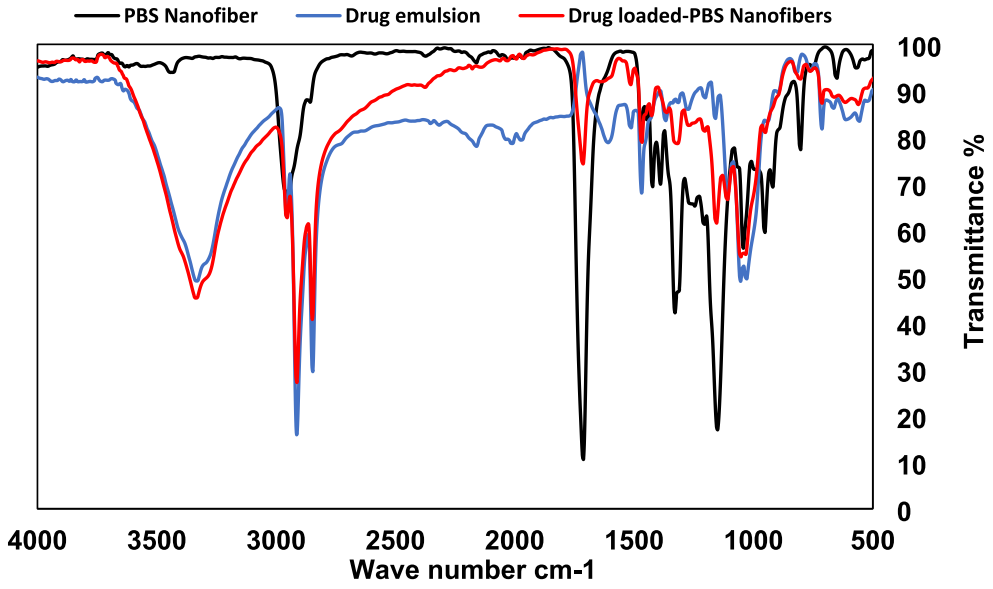

Fig. 6. FTIR chart of PBS nanofibers, drug emulsion, and nanofiber loaded with drug emulsion.

crystalline nature of both CNC and n-eicosan, where the sharp diffraction peaks allocating at 16.4°, 22.3° and 34.5° are assigned to the crystallographic structure cellulose I of CNC. The other diffraction peaks appearing at 19.5°, 19.8°, 23.5°, 24.8°, and 25.7° were related to the typical crystal planes of eicosan. On the other hand, by comparing with the XRD patterns of PBS nanofibers and emulsion, the drug-loaded PBS nanofibers displayed similar diffraction peaks accompanied by new sharp peaks appearing at 6.7°, 10.2°, 13.7°, and 17.23°, which is attributed to the drug molecules (α-amino phosphonate) [60].

3.6. Thermoresponsive drug release profile: DSC

The DSC technique can estimate the released drug from PBS-loaded drug/eicosan O/W emulsion [61]. Pure eicosan displays an endothermic melting peak at a maximum of 35–37 °C with enthalpy ranging about 247 J/g [62–64]. The eicosan undergoes a phase transition to the liquid at this latent heat melting point. Fig. 8 represents the DSC of PBS-loaded drug/emulsion compared to eicosan emulsion stabilized CNC and the pure PBS nanofibers.

It is witnessed from Fig. 8 that eicosan O/W emulsion and PBS-loaded drug/emulsion depicted a sharp melting point at a typical

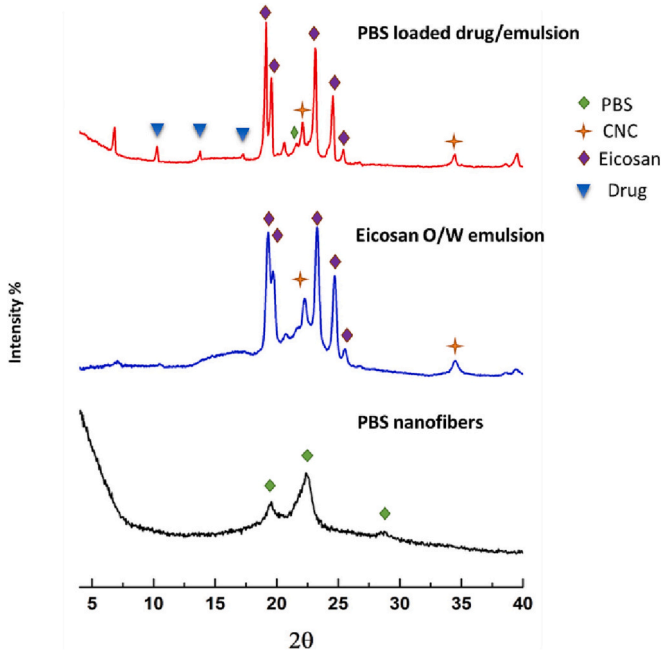

Fig. 7. XRD patterns of PBS nanofibers, eicosan O/W emulsion, and the drug-loaded PBS nanofibers.

eicosan melting range. These observations affirmed the thermal diffusion of loaded drug/emulsion from the PBS nanofiber mats at a temperature ranging from about 36–38 °C, which, in turn, renders the PBS nanofibers loaded drug/emulsion thermal responsive property close to the human body temperature. However, the thermograph of the PBS-loaded drug/emulsion showed a small peak area compared to that of the eicosan emulsion, which is attributed to the smaller eicosan content in the loaded PBS nanofiber. It can also be noticed from DSC thermograms that the thermal behavior of PBS-loaded drug/emulsion manifested a marginal shifting in the melting point, which attained its maximum value at around 37.5 °C compared to 39 °C of native eicosan emulsion. This could be due to the effect of drug mixing during the formation of drug emulsion and the use of a spry loading technique controlled by a specific drug/emulsion concentration. The release behavior of PBS-loaded drug/emulsion may be enhanced as the shift to a lower temperature close to the human body affects the responsibility of PBS nanofibers to reach their maxima at 37.5 °C instead of 39 °C, which is the preferred temperature for any proposed thermos-responsive system for drug release is equal to or higher than 37 °C (Ferreira, [65]). In context, the average outermost surface temperature of the human body (skin) ranges between 33.5 and 36.9C, though the skin's temperature is lower over the protruding organs, like the nose and ears, and higher overactive organs like muscles [66]. Herein, PBS nanofibers loaded drug tends to sustain drug release with a low dose to wound at average human body temperature 36 °C – 37 °C. The change in wound temperature often induced by pathogens leads to rapid drug release from the PBS nanofibers, which can be proposed as a suiTable vehicle for epidermal drug release control. Moreover, the exact concentration of loaded drug in PBS-loaded drug/emulsion is 2.7 % based on the ratio of melting enthalpy of the peaks area of emulsion and PBS-loaded drug/emulsion (drug:eicosan = 1:2).

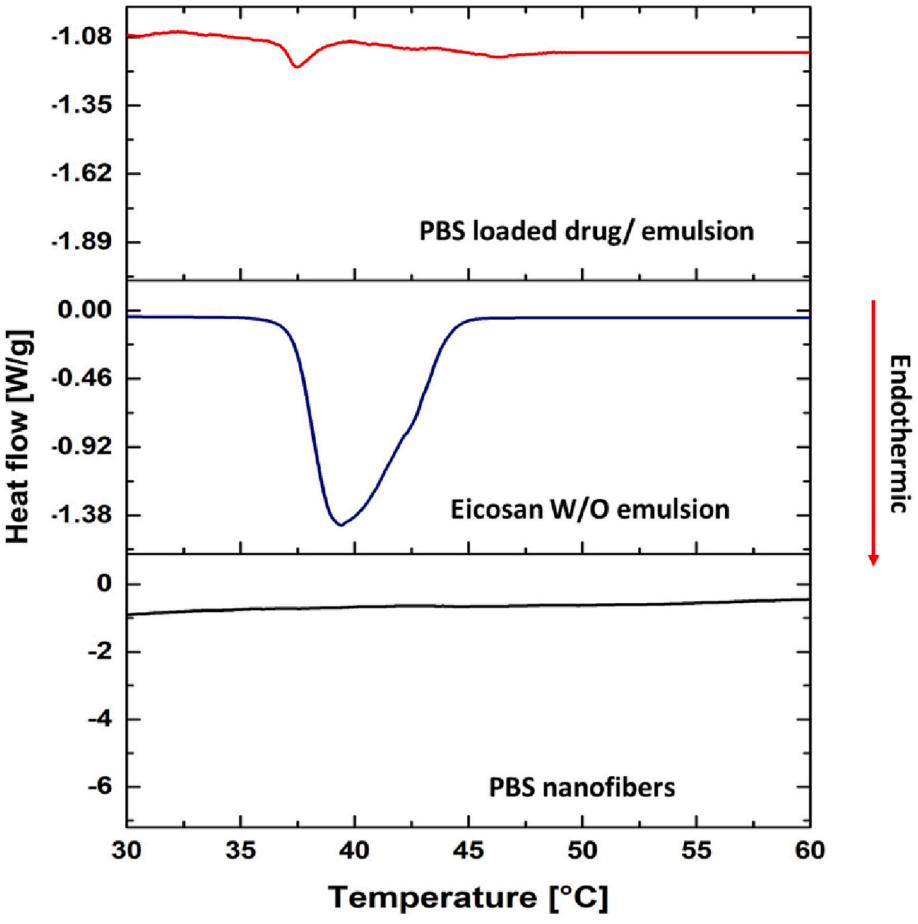

Fig. 8. DSC thermograms of the first heating of PBS nanofibers, eicosan O/W emulsion, and the drug-loaded PBS nanofibers.

Table 3
In vitro antimicrobial activity of coated nanofibers membrane discs of 23 mm diameter with active ingredient by agar diffusion method.

Microorganism inhibition zone diameter (mm)					
	Gram +ve bacteria		Gram –ve bacteria		Yeast
Incubation temperature	*Bacillus subtilis*	*Staphylococcus aureus*	*Escherichia coli*	*Klebsiella pneumonia*	*Candida albicans*
Pre-incubation at 25 °C	–	–	–	–	–
Pre-incubation at 39 °C	34 ± 1.7	30 ± 1.5	31 ± 1.55	30 ± 1.5	37 ± 1.85

3.7. Antimicrobial activity of treated nanofibers

The antimicrobial activity of the drug-emulsion-loaded nanofibers was investigated using the inhibition zone technique, and the results are presented in Table 3. Usually, tested samples are placed in the inoculated agar plates at room temperature for one hour to slow the bacterial growth and allow the release of loaded active materials on the surface of the agar. The plates are then incubated for 24 h at 35 °C before measuring the inhibition zone. However, in the current work, this method was modified to fit the mode of action of our thermoresponsive system. Nanofiber swatches (1 cm diameter) loaded with drug emulsion were placed in the inoculated agar plate and then preincubated at 39 °C for 15 min to mimic the infected body temperature (second-degree fever [67,68]) and ensure eicosan melting and the release of the hosted drug. All samples were found to be active against the tested microorganisms, and clear inhibition zones were observed, which means that the drug was released from the emulsion formulation and was still effective against the tested microbes. On the other hand, no inhibition zone was observed when the agar plates were preincubated at room temperature (25 °C).

4. Conclusions

Thermoresponsive wound dressings produced by semi-industrial scale needleless electrospinning of polybutylene succinate and loaded with biologically active antimicrobial α-aminophosphonate o/w emulsion were successfully fabricated. The results showed the wettability and thermoresponsive behavior of the drug-loaded mats. Moreover, all nanofiber mats loaded with various synthesized α-aminophosphonate derivatives showed antimicrobial properties against Gram-positive, Gram-negative, and yeast microorganisms as clear inhibition zones were observed. The results of this study demonstrated that the developed thermoresponsive antimicrobial wound dressings from renewable resources are excellent candidates as smart wound dressings for skin wound healing.

CRediT authorship contribution statement

Dalia Elsherbiny: Conceptualization, methodology.
Abdelrahman Abdelgawad: Conceptualization, methodology, writing.
Tharwat Shaheen: Methodology, investigation.
Nayera Abdelwahed: Methodology, writing.
Stefan Jockenhövel: Supervision, reviewing, editing.
Samaneh Ghazanfari: Supervision, reviewing, editing.

Declaration of competing interest

The authors declare that they have no known competing financial interests or personal relationships that could have appeared to influence the work reported in this paper.

Appendix A. Supplementary data

Supplementary data to this article can be found online at https://doi.org/10.1016/j.ijbiomac.2023.123655.

References

[1] W.R. Jarvis, Infection control and changing health-care delivery systems, Emerg. Infect. Dis. 7 (2) (2001) 170.
[2] J.P. Burke, Infection control — a problem for patient safety, N. Engl. J. Med. 7 (2003).
[3] B.B. Bonev, N.M. Brown, Bacterial Resistance to Antibiotics: From Molecules to Man, Wiley Online Library, 2019.
[4] S. Dhivya, et al., Wound dressings–a review, J. Biomed. 5 (4) (2015) 1–5.
[5] E. Rezvani Ghomi, et al., Wound dressings: current advances and future directions, J. Appl. Polym. Sci. 136 (27) (2019) 47738.
[6] A. Amira, et al., Recent advances in the synthesis of α-aminophosphonates: a review, ChemistrySelect 6 (24) (2021) 6137–6149.
[7] D.A. Elsherbiny, et al., Synthesis, antimicrobial activity, and sustainable release of novel α-aminophosphonate derivatives loaded carrageenan cryogel, Int. J. Biol. 163 (2020) 96–107.
[8] P. Kafarski, B. Lejczak, Aminophosphonic acids of potential medical importance, Curr. Med. Chem. Anticancer Agents 1 (3) (2001) 301–312.
[9] A.K. Mungara, in: Synthesis and Antiproliferative Activity of Novel α-aminophosphonates 60(12), 2012, pp. 1531–1537.
[10] P.R. Varga, G. Keglevich, Synthesis of α-aminophosphonates and related derivatives; the last decade of the kabachnik-fields reaction, Molecules 26 (9) (2021) 2511.
[11] J. Bueno, in: K. Kon, M. Rai (Eds.), Antimicrobial Strategies in Novel Drug Delivery Systems: Applications in the Treatment of Skin and Soft Tissue Infections. The Microbiology of Skin, Soft Tissue, Bone and Joint Infections 2, Academic Press, 2017, pp. 271–286.
[12] M.E. Aljghami, et al., Emerging innovative wound dressings, Ann. Biomed. Eng. 47 (3) (2019) 659–675.
[13] A. Jones, L. San Miguel, Are modern wound dressings a clinical and cost-effective alternative to the use of gauze? J. Wound Care 15 (2) (2006) 65–69.
[14] A. Abou-Okeil, et al., Wound dressing based on nonwoven viscose fabrics, Carbohydr. Polym. 90 (1) (2012) 658–666.
[15] B.A. Aderibigbe, B. Buyana, Alginate in wound dressings, Pharmaceutics 10 (2) (2018) 42.
[16] K. Varaprasad, et al., Alginate-based composite materials for wound dressing application: a mini review, Carbohydr. Polym. 236 (2020), 116025.
[17] W. Paul, C.P. Sharma, Chitosan and alginate wound dressings: a short review, Trends Biomater. Artif. Organs 18 (1) (2004) 18–23.
[18] C. Doillon, et al., Collagen-based wound dressings: control of the pore structure and morphology, J. Biomed. Mater. Res. 20 (8) (1986) 1219–1228.
[19] J. Stergar, U. Maver, Review of aerogel-based materials in biomedical applications, J. Sol-Gel Sci. Technol. 77 (3) (2016) 738–752.
[20] R.S. Ambekar, B. Kandasubramanian, Advancements in nanofibers for wound dressing: a review, Eur. Polym. J. 117 (2019) 304–336.
[21] M.E. El-Naggar, et al., Curdlan in fibers as carriers of tetracycline hydrochloride: controlled release and antibacterial activity, Carbohydr. Polym. 154 (2016) 194–203.
[22] S. Homaeigohar, A. Boccaccini, Antibacterial biohybrid nanofibers for wound dressings, Acta Biomater. 107 (2020) 25–49.
[23] T. Mirmajidi, et al., In vitro and in vivo evaluation of a nanofiber wound dressing loaded with melatonin, Int. J. Pharm. 596 (2021), 120213.
[24] A. Ghajarieh, et al., Biomedical applications of nanofibers, Russ. J. Appl. Chem. 94 (7) (2021) 847–872.
[25] S. Ramakrishna, An Introduction to Electrospinning and Nanofibers, World scientific, 2005.
[26] A. Ehrmann, Non-toxic crosslinking of electrospun gelatin nanofibers for tissue engineering and biomedicine—a review, Polymers 13 (12) (2021) 1973.
[27] D.S. Katti, et al., Bioresorbable nanofiber-based systems for wound healing and drug delivery: optimization of fabrication parameters, J. Biomed. Mater. Res. B Appl. Biomater. 70 (2) (2004) 286–296.
[28] G. Guidotti, et al., Regenerated wool keratin-polybutylene succinate nanofibrous mats for drug delivery and cells culture, Polym. Degrad. 179 (2020), 109272.
[29] M.-E. Ostheller, et al., Curcumin and silver doping enhance the spinnability and antibacterial activity of melt-electrospun polybutylene succinate fibers, Nanomaterials 12 (2) (2022) 283.
[30] Y. Fang, L. Xu, Four self-made free surface electrospinning devices for high-throughput preparation of high-quality nanofibers, Beilstein J. Nanotechnol. 10 (1) (2019) 2261–2274.
[31] Z. Shao, et al., High-throughput fabrication of quality nanofibers using a modified free surface electrospinning, Nanoscale Res. Lett. 12 (1) (2017) 1–9.
[32] R. Ramakrishnan, et al., Needleless electrospinning technology–an entrepreneurial perspective, Indian J. Sci. 9 (15) (2016) 2–11.

[33] I. Partheniadis, et al., A mini-review: needleless electrospinning of nanofibers for pharmaceutical and biomedical applications, Processes 8 (6) (2020) 673.
[34] Antibiotic Resistance, World Health Organization Website, 2020.
[35] J.L. Frandsen, H. Ghandehari, Recombinant protein-based polymers for advanced drug delivery, Chem. Soc. Rev. 41 (7) (2012) 2696–2706.
[36] M.A. Da Silva, Engineering thermoresponsive emulsions with branched copolymer surfactants, Macromol. Mater. Eng. 203 (10) (2022) 2200321.
[37] I. Capron, B. Cathala, Surfactant-free high internal phase emulsions stabilized by cellulose nanocrystals, Biomacromolecules 14 (2) (2013) 291–296.
[38] K. Ganguly, et al., TEMPO-cellulose nanocrystal-capped gold nanoparticles for colorimetric detection of pathogenic DNA, ACS Omega 6 (19) (2021) 12424–12431.
[39] S. Stubbs, et al., A review on the synthesis of bio-based surfactants using green chemistry principles, DARU J. Pharm. Sci. (2022) 1–20.
[40] I. Capron, et al., Behavior of nanocelluloses at interfaces, Curr. Opin. Colloid Interface Sci. 29 (2017) 83–95.
[41] S. Llàcer Navarro, et al., The effect of sulfate half-ester groups on cellulose nanocrystal periodate oxidation, Cellulose 28 (15) (2021) 9633–9644.
[42] S.P. Bangar, et al., Surface modifications of cellulose nanocrystals: processes, properties, and applications, Food Hydrocoll. 130 (2022), 107689.
[43] S.S. Deveci, G. Basal, Preparation of PCM microcapsules by complex coacervation of silk fibroin and chitosan, Colloid Polym. Sci. 287 (12) (2009) 1455–1467.
[44] U. Yucel, et al., Solute distribution and stability in emulsion-based delivery systems: an EPR study, J. Colloid Interface Sci. 377 (1) (2012) 105–113.
[45] T.I. Shaheen, I. Capron, Formulation of re-dispersible dry o/w emulsions using cellulose nanocrystals decorated with metal/metal oxide nanoparticles, RSC Adv. 11 (51) (2021) 32143–32151.
[46] D.C. Das, et al., Antibacterial activity and phytochemical analysis of Cardanthera difformis Druce leaf extracts from West Bengal, India, Int. J. Phytorem. 5 (4) (2013) 446.
[47] F. Elmi, et al., The use of antibacterial activity of ZnO nanoparticles in the treatment of municipal wastewater, Water Sci. Technol. 70 (5) (2014) 763–770.
[48] R. Aissa, et al., New promising generation of phosphates α-aminophosphonates: design, synthesis, in-vitro biological evaluation and computational study, J. Mol. Struct. 1247 (2022), 131336.
[49] M. Rostamizadeh, et al., A novel and efficient synthesis of α-aminophosphonates by use of triphenyl phosphite in acetic acid media, Phosphorus Sulfur Silicon 186 (2) (2011) 334–337.
[50] T. Abudula, et al., Electrospun cellulose Nano fibril reinforced PLA/PBS composite scaffold for vascular tissue engineering, J. Polym. Res. 26 (5) (2019) 1–15.
[51] E.H. Jeong, et al., Electrospinning and structural characterization of ultrafine poly (butylene succinate) fibers, Polymer 46 (23) (2005) 9538–9543.
[52] N. Stoyanova, et al., Poly(l-lactide) and poly(butylene succinate) immiscible blends: from electrospinning to biologically active materials, Mater. Sci. Eng. C 41 (2014) 119–126.
[53] C. Thompson, et al., Effects of parameters on nanofiber diameter determined from electrospinning model, Polymer 48 (23) (2007) 6913–6922.
[54] N. Karakehya, Comparison of the effects of various reinforcements on the mechanical, morphological, thermal and surface properties of poly (butylene succinate), Int. J. Adhes. Adhes. 110 (2021), 102949.
[55] A.S. Pakdel, et al., Cellulose nanocrystal (CNC)–latex nanocomposites: effect of CNC hydrophilicity and charge on rheological, mechanical, and adhesive properties, Macromol. Rapid Commun. 42 (3) (2021), 2000448.
[56] K. Sun, et al., The design of phase change materials with carbon aerogel composites for multi-responsive thermal energy capture and storage, J. Mater. Chem. A 9 (2) (2021) 1213–1220.
[57] B. Abderrahim, et al., Kinetic thermal degradation of cellulose, polybutylene succinate and a green composite: comparative study, World J. Environ. Eng. 3 (4) (2015) 95–110.
[58] L.É. Uhljar, et al., In vitro drug release, permeability, and structural test of ciprofloxacin-loaded nanofibers, Pharmaceutics 13 (4) (2021) 556.
[59] P. Shaiju, et al., Biodegradation of poly (butylene succinate)(PBS)/stearate modified magnesium-aluminium layered double hydroxide composites under marine conditions prepared via melt compounding, Molecules 25 (23) (2020) 5766.
[60] M.E. Mahmoud, et al., Development of titanium oxide-bound-α-aminophosphonate nanocomposite for adsorptive removal of lead and copper from aqueous solution, Water Resour. Ind. 23 (2020), 100126.
[61] B. Singh, et al., Development, optimization, and characterization of polymeric electrospun nanofiber: a new attempt in sublingual delivery of nicorandil for the management of angina pectoris, Artif. Cells Nanomed. Biotechnol. 44 (6) (2016) 1498–1507.
[62] D.G. Atinafu, et al., Introduction of eicosane into biochar derived from softwood and wheat straw: influence of porous structure and surface chemistry, Chem. Eng. J. 415 (2021), 128887.
[63] L. Che Rose, et al., A SPION-eicosane protective coating for water soluble capsules: evidence for on-demand drug release triggered by magnetic hyperthermia, Sci. Rep. 6 (1) (2016) 1–5.
[64] J.C. van Miltenburg, et al., Heat capacities and derived thermodynamic functions of n-nonadecane and n-eicosane between 10 K and 390 K, J. Chem. Eng. Data 44 (4) (1999) 715–720.
[65] N.N. Ferreira, et al., Recent advances in smart hydrogels for biomedical applications: from self-assembly to functional approaches, Eur. Polym. J. 99 (2018) 117–133.
[66] W. Bierman, The temperature of the skin surface, J. Am. Med. Assoc. 106 (14) (1936) 1158–1162.
[67] D. Ogoina, Fever, fever patterns and diseases called 'fever'–a review, J. Infect. Public Health 4 (3) (2011) 108–124.
[68] N. Tang, et al., Wearable sensors and systems for wound healing-related ph and temperature detection, Micromachines 12 (4) (2021) 430.